

Gluon saturation and baryon stopping in the SPS, RHIC, and LHC energy regions

Shuang Li¹ and Sheng-Qin Feng^{1,2,3}

¹*College of Science, China Three Gorges University, Yichang 443002, China*

²*Key Laboratory of Quark and Lepton Physics (Huazhong Normal Univer.), Ministry of Education Wuhan 430079 China and*

³*School of Physics and Technology, Wuhan University, Wuhan 430072, China*

A new geometrical scaling method with gluon saturation rapidity limit is proposed to study the gluon saturation feature of central rapidity region of relativistic nuclear collisions. The net-baryon number is essentially transported by valence quarks that probe the saturation regime in the target by multiple scattering. We take advantage of the gluon saturation model with geometric scaling of rapidity limit to investigate the net baryon distributions, nuclear stopping power and gluon saturation feature in the SPS and RHIC energy regions. Predications for the net-baryon rapidity distributions, the mean rapidity loss and gluon saturation feature in central Pb + Pb collisions at LHC are made in this paper.

Keywords: gluon saturation, geometrical scaling, net-baryon distributions

PACS numbers: 25.75.-q, 25.75.Ag, 25.75.Nq

I. INTRODUCTION

During the relativistic heavy-ion collisions, the fast valence quarks in one nucleus scatter in the other nucleus by exchanging soft gluons, leading to their redistribution in rapidity space. The net-baryon number is essentially transported by valence quarks that probe the saturation regime in the target by multiple scattering.

Experimental heavy-ion investigations at the Large Hadron Collider (LHC) pay much more attention to the mid-rapidity region since ALICE covers rapidity up to $|y| = 2$. It provides measurements of lower x than before at energy scale that is high enough to provide crucial tests of gluon saturation. Therefore LHC will provide more opportunities to study the gluon saturation feature at small x .

At very high energies or small values of Bjorken variable x , the density of partons per unit transverse area, in nucleon or nucleus becomes so large that it would lead to a gluon saturation of partonic distribution. The existence of this phenomenon was confirmed in the experiments at HERA [1, 2]. The typical results from the experiments contain two parts: the small x problem and the geometric scaling. It was predicted by an effective theory, the CGC (Color Glass Condensate), which describes the behavior of the small x components of the hadronic wave function in QCD. In this paper, we use this CGC theory to discuss the questions of nuclear stopping and gluon saturation in relativistic heavy-ion collisions at SPS, RHIC and LHC.

The kinetic energy of the relativistic heavy-ion collisions that is removed from the beam and which is available for the production of a state such as the QGP (quark gluon plasma) depends on the amount of stopping between the colliding ions. The stopping can be estimated from the rapidity loss experienced by the baryons in the colliding nuclei [3–9]. If the incoming beam baryons have rapidity, y_b relative to the CM (which has $y = 0$) and average rapidity

$$\langle y \rangle = \frac{\int_0^{y_b} y dy dN/dy}{\int_0^{y_b} dy dN/dy} \quad (1)$$

the average rapidity loss is

$$\langle \delta y \rangle = y_b - \langle y \rangle \quad (2)$$

Here dN/dy denotes the number of net-baryons (number of baryons minus the number of anti-baryons) per unit of rapidity. The studies of net baryon distributions and nuclear stopping have been discussed by non-uniform collective flow model [10–13]. We will use gluon saturation to study net-baryon in this paper.

Here we should mention a novel gluon saturation model proposed by Yacine Mehtar-Tani and Georg Wolschin [14, 15]. An analytical scaling law is derived within the color glass condensate framework based on small-coupling QCD in this model. Inspired by this model [14, 15], we study the net baryon distributions of central collisions in the SPS and RHIC energy regions by introducing the effective quark mass and rapidity limit of gluon saturation region. Here we use a new geometric scaling method to define the rapidity limit of gluon saturation region. The important difference is the definition of geometric scaling between our model and Ref.[14,15]. It realized [14, 15] that the geometric scaling is mainly about the peak positions of net-baryon rapidity distribution. But our model realizes the geometric scaling of net-baryon rapidity distribution is mainly about the gluon saturation rapidity limit. The net-baryon rapidity distributions and the mean rapidity loss in central Pb + Pb collisions at LHC are predicted in this paper.

II. GLUON SATURATION MODEL WITH GEOMETRIC SCALING

The ideas for the color glass condensate are motivated by HERA data on the gluon distribution function [1].

The gluon density, $xG(x, Q^2)$, rises rapidly as a function of decreasing fractional momentum, x , or increasing resolution Q . This rise in the gluon density ultimately owes its origin to the non-Abelian nature of QCD and that the gluons carry color charge. At higher and higher energies, smaller x and larger Q become kinematics accessible. The rapid rise with $\ln(1/x)$ was expected in a variety of theoretical works [14–23]. Due to the intrinsic non-linearity of QCD, gluon showers generate more gluon showers producing an exponential avalanche toward small x . The physical consequence of this exponential growth is that the density of gluons per unit area per unit rapidity of any hadrons including nuclei must increase rapidly as x decreases [14, 15].

The net-baryon number of relativistic heavy ion collisions is essentially transported by valence quarks that probe the saturation regime in the target by multiple scatterings. During the relativistic heavy ion collisions, the fast valence quarks in one nucleus scatter in the other nucleus by exchanging soft gluons, leading to their redistribution in rapidity space. The valence quark parton distribution at large x is well known, which corresponds to the forward and backward rapidity region, to access the gluon distribution at small x in the target nucleus. Therefore, this picture provides a clean probe of the gluon distribution, $\varphi(x, p_T)$, at small x in the saturation regime.

For symmetric heavy ion collisions, the contribution of the fragmentation of the valence quarks in the projection is given by the simple formula for the rapidity distribution of interactions with gluon in the target [14, 15]

$$\frac{dN}{dy} = \frac{C}{(2\pi)^2} \int \frac{d^2 p_T}{p_T^2} x_1 q_v(x_1) \varphi(x_2, p_T) \quad (3)$$

here $x_1 q_v(x_1)$ is the valence quark distribution of a nucleus, $\varphi(x_2, p_T)$ is the gluon distribution of another nucleus, p_T is the transverse momentum of the produced quark and y its rapidity. One important prediction of the gluon saturation with geometric scaling is the geometric scaling: the gluon distribution depends on x and p_T only through the scaling variable $p_T^2/Q_s^2(x)$, here $Q_s^2(x) = A^{1/3} Q_0^2 x^{-\lambda}$. Geometric scaling was confirmed experimentally at HERA [1]. The fit value $\lambda = 0.2 - 0.3$ agrees with theoretical estimates based on next-to-leading order Balitskii-Fadin-Kuraev-Lipatov (BFKL) results [24–26].

The longitudinal momentum fractions carried, respectively, by the valence quark in the projectile and the soft gluon in the target are $x \equiv x_1 = (p_T/\sqrt{s}) \exp(y)$, and $x_2 = (p_T/\sqrt{s}) \exp(-y)$. Then we can deduce the relation as follows [14, 15]

$$x \equiv x_1, \quad x_2 = x e^{-2y}, \quad p_T^2 = x^2 s e^{-2y} \quad (4)$$

The gluon distribution is defined as

$$\varphi(x_2, p_T) = \varphi\left(\frac{p_T^2}{Q_s^2(x_2)}\right) = 4\pi \cdot \frac{p_T^2}{Q_s^2(x_2)} \cdot \exp\left(-\frac{p_T^2}{Q_s^2(x_2)}\right) \quad (5)$$

When we use the variables as Eq.4, we can take the relation as follows

$$\frac{p_T^2}{Q_s^2(x_2)} = \frac{(x \cdot \sqrt{s} \cdot e^{-y})^2}{A^{1/3} Q_0^2 x_2^{-\lambda}} = \frac{x^{2+\lambda}}{e^{2(1+\lambda)y}} \cdot \frac{s}{Q_0^2} \cdot \frac{1}{A^{1/3}} \quad (6)$$

If we make $\frac{p_T^2}{Q_s^2(x_2)} = x^{2+\lambda} \cdot e^\tau$ from Eq.6 we can take

$$e^\tau = \frac{1}{e^{2(1+\lambda)y}} \cdot \frac{s}{Q_0^2} \cdot \frac{1}{A^{1/3}} \quad (7)$$

and a geometrical scaling with rapidity is introduced as

$$\tau = \ln\left(\frac{s}{Q_0^2}\right) - \ln A^{1/3} - 2(1+\lambda)y \quad (8)$$

Thus Eq.3 is given as follows

$$\frac{dN}{dy} = \frac{C}{2\pi} \int_0^1 \frac{dx}{x} x q_v(x) \varphi(x^{2+\lambda}, e^\tau) \quad (9)$$

As mentioned before, the dependence of τ on y in Ref.[14,15] is related to the peak position, but here we use the dependence of τ on y to define the rapidity limit of gluon saturation. A rapidity variable is introduced in Eq.8 to discuss the gluon saturation rapidity region. The rapidity limit variable y is

$$y = \frac{1}{1+\lambda} (y_b - \ln A^{1/6}) + \frac{1}{2(1+\lambda)} \left(\ln \frac{m_n^2}{Q_0^2} - \tau \right) \quad (10)$$

here $y_b \approx \ln(\sqrt{s}/m_n)$ is the beam rapidity with nucleon mass m_n . It usually defines $x \leq 0.01$ as a small x region, and in this region, it is taken as the gluon saturation region. By taking $\tau = \ln(1/x)|_{x=0.01}$, we can figure out the rapidity region of gluon saturation as follows

$$\begin{aligned} y_{\text{saturation}} &= \frac{1}{1+\lambda} (y_b - \ln A^{1/6}) + \frac{1}{2(1+\lambda)} \left(\ln \frac{m_n^2}{Q_0^2} - \tau|_{x=0.01} \right) \end{aligned} \quad (11)$$

The gluon distribution is

$$\varphi(x_2, p_T) = \begin{cases} \text{const} & (x < 0.01) \\ 4\pi \frac{p_T^2}{Q_s^2(x_2)} \cdot e^{-\frac{p_T^2}{Q_s^2(x_2)}} \cdot (1-x_2)^4 & (x > 0.01) \end{cases} \quad (12)$$

The valence quarks distribution is

$$x q_v(x) = \begin{cases} \propto x^{0.5} & (x < 0.01) \\ \propto (x u_v + x d_v) & (x > 0.01) \end{cases} \quad (13)$$

So the net-baryon distribution which originates from the projectile is

$$\frac{dN}{dy} = \begin{cases} \propto \exp\left\{\frac{1+\lambda}{2+\lambda}y\right\} & (0 \leq y \leq y_{\text{saturation}}) \\ \propto \int_{0.01}^1 \frac{dx}{x} (x u_v + x d_v) 4\pi \cdot \frac{p_T^2}{Q_s^2(x_2)} \cdot \exp\left\{-\frac{p_T^2}{Q_s^2(x_2)}\right\} \cdot (1-x_2)^4 & (y > y_{\text{saturation}}) \end{cases} \quad (14)$$

The contribution of valence quarks in the other beam nucleus is added incoherently by changing $y \rightarrow -y$. The total rapidity distributions of the symmetry interaction systems are the summation of the contributions from the projectile and target, respectively

$$\frac{dN}{dy}|_{total} = \frac{dN}{dy}(y) + \frac{dN}{dy}(-y) \quad (15)$$

Compared with Ref.[14,15], we will introduce effective dynamic quark mass in this paper by substituting the transverse momentum p_T as $\sqrt{(x\sqrt{s}e^{-y})^2 - m^2}$, i.e. $p_T = \sqrt{(x\sqrt{s}e^{-y})^2 - m^2}$ here m is the dynamic quark mass, which was given by baryon mass in Ref.[14,15]. The detailed study of dynamic mass with collision energies will be given in the next section.

III. THE NET BARYON DISTRIBUTIONS IN THE SPS TO LHC ENERGY REGIONS

The integrated net-proton rapidity distributions are scaled by a factor of 2.05 [2] to obtain the net-baryon distributions. The rapidity distributions of net baryon for different energies of relativistic heavy nuclear collisions (Pb + Pb and Au + Au) at SPS and RHIC are given in Figure 1.

The estimated numbers of participants are 390, 315, and 357 for $\sqrt{s_{NN}} = 17.3, 62.4$, and 200 GeV, respectively. The solid circles correspond to the experimental result of central collisions [3–9], and the real lines are the calculated results from the gluon saturation model with geometric scaling. It is found that our model describes the experimental data of net-baryon distributions very well when we discuss Pb-Pb center collisions at the SPS energy region and Au-Au center collisions at the RHIC energy region. The $\lambda = 0.2$ and $Q_0^2 = 0.05 \text{ GeV}^2$ are fixed in our whole calculations.

We show in Fig.2 the computation resulting from our discussions, the centrality dependence of the rapidity distribution at $\sqrt{s_{NN}} = 200 \text{ GeV}$. The estimated numbers of participants are 280, 200, 114 and 54 for centralities of 0%–10%, 10%–20%, 20%–40%, and 40%–60% (from top to bottom) in Au+Au collisions at RHIC energies of $\sqrt{s_{NN}} = 200 \text{ GeV}$, respectively.

By studying the experimental results with our model, we may get the conclusion for the net-baryon distribution from SPS to LHC as follows: 1) The gluon saturation model with geometric scaling may be a good theory to study net-baryon distribution at central collisions at SPS and RHIC. The contributions of spectator nucleons can be neglected when considering only the central collisions. The gluon saturation feature of central rapidity can be studied from our discussion. The values of central rapidity of gluon saturation ($y_{saturation}$) are 1.06, 2.013 and 3.10 from Eq.11 for $\sqrt{s_{NN}} = 17.3, 62.4$, and 200 GeV, respectively.

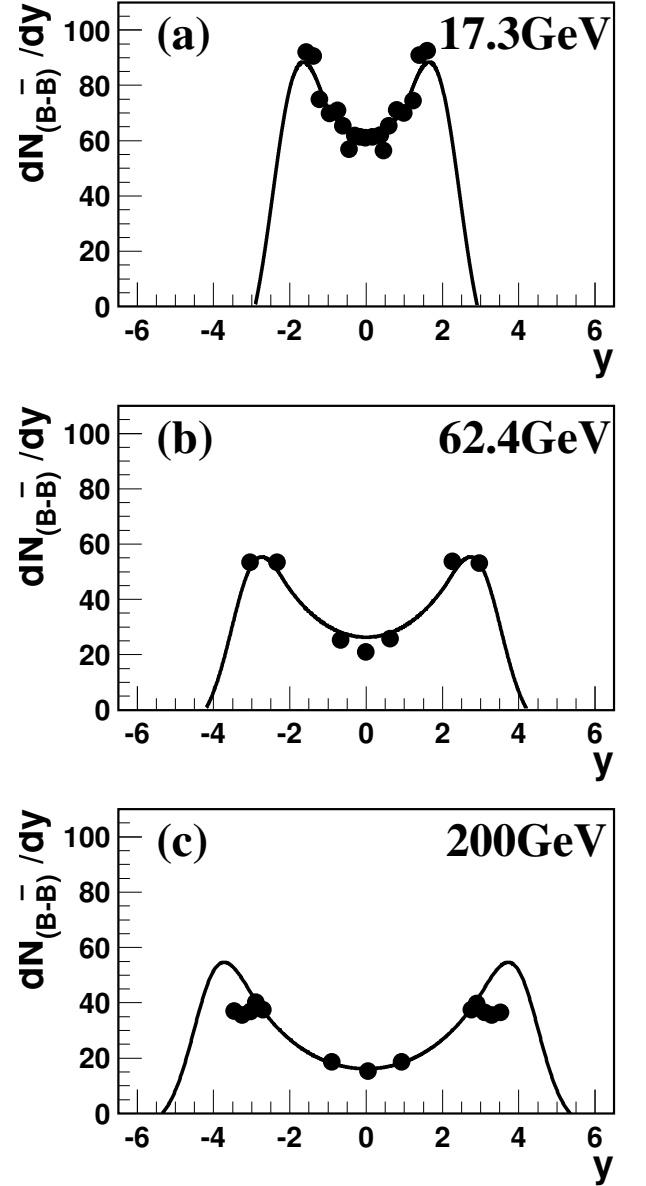


FIG. 1: Net-Baryon distributions of central collisions at SPS $\sqrt{s_{NN}} = 17.3 \text{ GeV}$ of Pb-Pb interactions and at RHIC $\sqrt{s_{NN}} = 62.4$ and 200 GeV of Au-Au interactions; the experimental results are from [3–9].

(2) The net baryon rapidity distribution in central Pb+Pb collisions at LHC energies of $\sqrt{s_{NN}} = 5.52 \text{ TeV}$ is predicted by gluon saturation model with geometric scaling. The theoretical distribution is shown in Fig.3 for $y_{saturation} = 5.86$. The gluon saturation region is larger than those of RHIC and SPS. It is found that the separation of two symmetric peaks of net-baryon is much wider than that of SPS and RHIC.

(3) The mean rapidity loss $\langle \delta y \rangle = y_b - \langle y \rangle$ is shown in Fig. 4. We show that the dependence of mean rapidity loss increase on y_b as

$$\langle \delta y \rangle = 1.548 \cdot \ln(y_b) + 0.036 \quad (16)$$

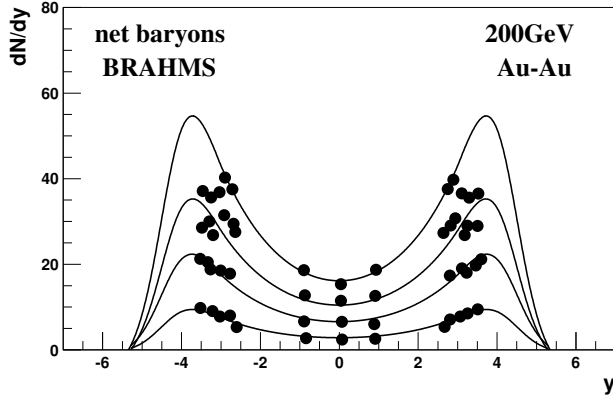


FIG. 2: Rapidity distributions of net baryons at different centrality; the experimental results are from [27], and the real lines are from our model.

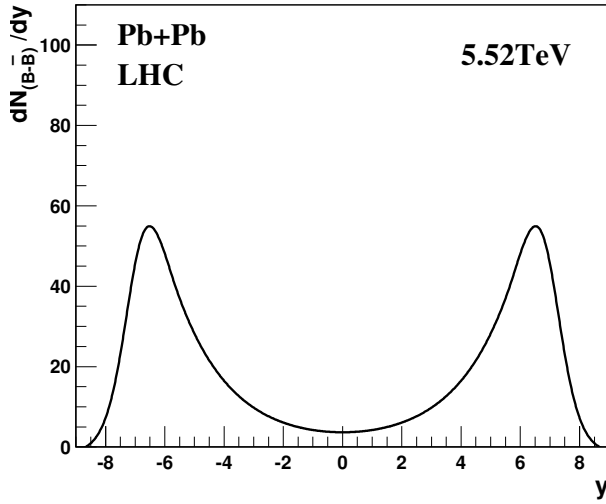


FIG. 3: The rapidity distribution of net baryons in central Pb+Pb collisions at LHC energies of $\sqrt{s_{NN}} = 5.52$ TeV. The theoretical distribution is from our discussion.

In Figure.4, the star (*) is our prediction result of the mean rapidity loss $\langle \delta y \rangle$ for Pb + Pb central collisions at LHC energies of $\sqrt{s_{NN}} = 5.52$ TeV ($y_b = 8.68$). In high-energy central nucleus-nucleus collisions, the baryon matter will be slowed down and will lose a few units of rapidity. The term "nuclear stopping power" was introduced in high-energy nucleus-nucleus collisions by Busza and Goldhaber to refer to the degree of stopping an incident nucleon suffers when it impinges on the nuclear matter of another nucleus. Usually the mean rapidity loss $\langle \delta y \rangle = y_b - \langle y \rangle$ was used to represent the nuclear stopping power of nucleus -nucleus collisions.

(4) It is shown in Fig.5 that the dependence of percentage ratios of the net-baryon production from the central gluon saturation region on incident energy at $\sqrt{s_{NN}} = 17.3, 62.4, 200$ and 5520 GeV. It is found that the percentage ratio from the central gluon saturation region increases with the increase of the colliding

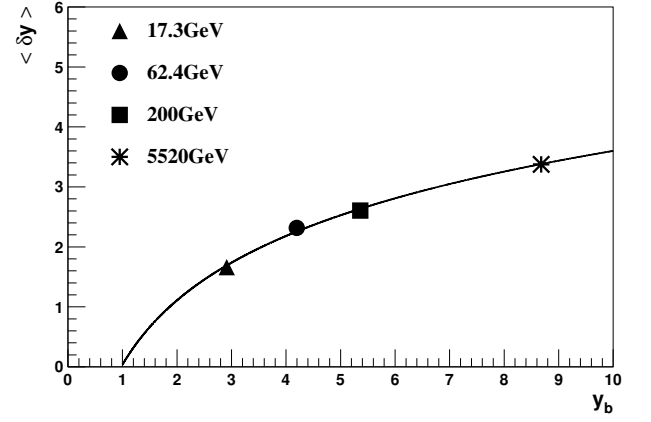


FIG. 4: The dependence of mean rapidity loss $\langle \delta y \rangle$ on beam rapidity y_b . The $\blacktriangle, \bullet, \blacksquare, *$ are the calculated results by our discussion for $\sqrt{s_{NN}} = 17.3, 62.4, 200$ and 5520 GeV, respectively. The real curve is the fit curve with $\langle \delta y \rangle = 1.548 \cdot \ln(y_b) + 0.036$

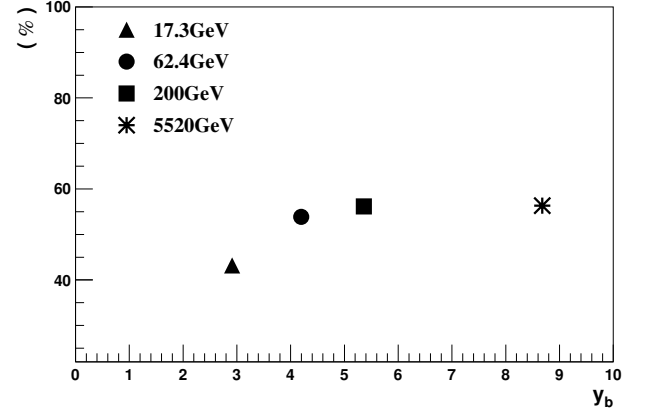


FIG. 5: The dependence of the percentage of net-baryon from the central gluon saturation region on the colliding energies at $\sqrt{s_{NN}} = 17.3, 62.4, 200$ and 5520 GeV.

energies. The percentage ratio from the saturation region rises rapidly from SPS $\sqrt{s_{NN}} = 17.3$ GeV to RHIC $\sqrt{s_{NN}} = 62.4$ GeV, but slowly from RHIC $\sqrt{s_{NN}} = 200$ GeV to LHC $\sqrt{s_{NN}} = 5520$ GeV. It is found that the percentage ratio is 43.17% at $\sqrt{s_{NN}} = 17.3$ GeV, but 56.31% at $\sqrt{s_{NN}} = 5520$ GeV. It seems that that the number of more than half of the net baryon at LHC comes from the central gluon saturation region.

5The dependence of the effective quark mass m_q on incident projective rapidity in the CMS at $\sqrt{s_{NN}} = 17.3, 62.4, 200$ and 5520 GeV is shown in Fig.6. It is found that the effective quark mass m_q varies slowly with the varying of the incident energies, and m_q varies among 0.24 to 0.26.

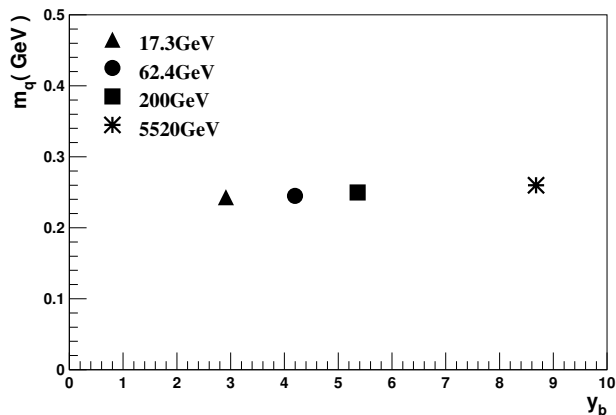


FIG. 6: The dependence of the effective quark mass on incident projective rapidity in the CMS at $\sqrt{s_{NN}} = 17.3, 62.4, 200$ and 5520 GeV.

IV. SUMMARY AND CONCLUSION

As discussed in Ref. [14,15], two distinct and symmetric peaks with respect to rapidity y occur at SPS energies and beyond in A + A collisions. A geometrical scaling feature of peak position of net baryon rapidity distributions was proposed to discuss about the net-baryon distribution [14, 15]. The rapidity separation between the peaks increases with energy and decreases with the increasing mass number, A , reflecting larger baryon stopping for heavier nuclei, as was investigated phenomenologically in the Non-uniform Flow Model (NUFM) [10–13]. In this work we show the geometrical scaling with gluon saturation rapidity limit, and also discuss the net-baryon rapidity distribution feature in the SPSRHIC and LHC.

A saturation model for net-baryon distributions that successfully describes the net-baryon rapidity distributions and their energy dependence is presented in this paper. The remarkable feature of geometric scaling predicted by our discussion is reflected in the net-baryon rapidity distribution, providing a direct test of gluon sat-

uration rapidity and x regions. The gluon saturation model is proposed by introducing a rapidity variable with gluon saturation region to define the gluon saturation region of central rapidity region of centrally colliding heavy ions at ultra-relativistic energies.

The gluon saturation features of central rapidity at SPS and RHIC can be investigated. It is found that the values of central rapidity of gluon saturation region increase with colliding energy. The detailed dependence of rapidity ($y_{saturation}$) of central gluon saturation on colliding energy is also investigated in this paper. We also predict the net baryon rapidity distribution in central Pb+Pb collisions at LHC energies of $\sqrt{s_{NN}} = 5.52 TeV$ by gluon saturation model with geometric scaling. The gluon saturation region is larger than those of RHIC and SPS, and the separation of two symmetric peaks of net-baryon is much wider than that of SPS and RHIC.

It is shown that gluon saturation feature is an important feature with the increasing of colliding energy. It seems that more than half of the produced net baryon numbers (56.31%) at LHC come from the central gluon saturation region, but the percentage ratio is 43.17% at SPS $\sqrt{s_{NN}} = 17.3 GeV$.

The dependencies of the percentage of net-baryon from the central gluon saturation region and stopping power on colliding energies are also studied in this paper. It is also found that the mean rapidity loss shows a linear dependence on $\ln(y_b)$. From that we can predict the mean rapidity loss for future LHC experimental data.

V. ACKNOWLEDGMENTS

This work was supported by National Natural Science Foundation of China (10975091), Excellent Youth Foundation of Hubei Scientific Committee (2006ABB036) and Education Commission of Hubei Province of China (Z20081302). The authors is indebted to Prof. Lianshou Liu for his valuable discussions and very helpful suggestions.

-
- [1] Breitweg J et al. Eur. Phys. J. C, 1999, 7: 609
 - [2] Iancu E, McLerran M. Phys. Lett. B, 2001, 510: 145
 - [3] Arsene I C et al. Phys. Lett. B, 2009, 677: 267
 - [4] Bearden I G et al. Phys. Rev. Lett., 2004, 93: 102301
 - [5] Klay J L et al. Phys. Rev. Lett., 2002, 88: 102301
 - [6] Bearden I G et al. Phys. Rev. Lett., 2005, 94: 162301
 - [7] Barrette J et al. Phys. Rev. C, 2000, 62: 024901
 - [8] Ahle L et al. Phys. Rev. C, 1999, 60: 064901
 - [9] Appelshauser H et al. Phys. Rev. Lett., 1999, 82: 2471
 - [10] FENG Shengqin, LIU Feng, LIU Lianshou. Phys. Rev. C, 2000, 63: 014901
 - [11] FENG Shengqin, YUAN Xianbao, SHI Yafei. Modern Phys Lett A, 2006, 21: 663
 - [12] FENG Shengqin, XIONG Wei. Phys. Rev. C, 2008, 77: 044906
 - [13] FENG Shengqin, YUAN Xianbao. Science in China Series G, 2009, 52: 198
 - [14] Mehtar-Tani Y et al. Phys. Rev. C, 2009, 80: 054905
 - [15] Mehtar-Tani Y et al. Phys. Rev. Lett., 2009, 102: 182301
 - [16] Gribov L V et al. Phys. Rep., 1983, 100: 1
 - [17] Mueller A H, Qiu J W. Nucl. Phys. B, 1986, 268: 427
 - [18] McLerran L, Venugopalan R. Phys. Rev. D, 1994, 50: 2225
 - [19] Kharzeev D et al. Nucl. Phys. A, 2005, 747: 60
 - [20] Kharzeev D, Levin E. Phys. Lett. B, 2001, 523: 79
 - [21] Kharzeev D et al. Phys. Lett. B, 2004, 599: 23
 - [22] Baier R et al. 2006, Nucl. Phys. A., 764: 515
 - [23] Triantafyllopoulos D N. Nucl. Phys. B, 2003, 648: 293

- [24] Kuraev E A et al. Sov. Phys. JETP, 1977, 45: 199
- [25] Ya.Ya.Balitsky et al. Sov. J. Nucl. Phys, 1978, 28: 822
- [26] Lipatov L N. Sov. J. Nucl. Phys. 1976, 23: 338
- [27] Debbé R et al. J. Phys.G. 2008, 35: 104004